Bulletin of the Seismological Society of America, Vol. 94, No. 6B, pp. S278–S292, December 2004

The 2002 Denali Fault and 2001 Kunlun Fault Earthquakes: Complex Rupture Processes of Two Large Strike-Slip Events

by A. Arda Ozacar and Susan L. Beck

Abstract We studied the source processes of two large continental earthquakes, the 3 November 2002 Denali fault earthquake and the 14 November 2001 Kunlun fault earthquake, associated with strike-slip faulting along ancient sutures. We inverted teleseismic *P* waveforms using a pulse-stripping method for multiple time windows with different focal mechanisms and derived composite source models. According to our results, the 2002 Denali fault earthquake began with initial thrusting (M_w 7.3) along a 40-km-long segment of the north-northwest-dipping Susitna Glacier fault and later ruptured a 300-km-long segment along the Denali and Totschunda faults with a right-lateral strike-slip mechanism (M_w 7.7). In contrast, the 2001 Kunlun fault earthquake nucleated near an extensional step-over with a subevent pair consisting of 30-km-long strike-slip (M_w 6.9) event and 40-km-long normal (M_w 6.8) faulting event and later ruptured a 350-km-long segment along the Kunlun fault with a left-lateral strike-slip mechanism (M_w 7.7). Both earthquakes propagated primarily unilaterally to the east and released most of their energy along slip patches (asperities) far from the hypocenter locations. We find that both the Denali fault and Kunlun fault earthquakes had high-average rupture velocities of 3.2 km/sec and 3.4 km/sec, respectively. We also compared the source properties of these two earthquakes with other strike-slip earthquakes. For scaling purposes, large strike-slip earthquakes were classified as interplate, oceanic intraplate, or continental intraplate events. By using this classification the Denali fault and Kunlun fault earthquakes have an interplate signature that suggests overall weak faulting.

Introduction

Continental strike-slip faults are often major sources for seismic hazard, but only a few large ($M_w \geq 7.5$) earthquakes along these faults have been studied with modern instrumentation. Understanding the nature of such large strike-slip earthquakes may ultimately help to reveal the underlying mechanics of the rupture process and allow better strong-motion predictions. The strong directivity associated with some large strike-slip earthquakes often contributes to increased damage.

Seismic analyses of many large strike-slip earthquakes suggest a multiple-event nature with complicated space-time functions of slip accommodated by complex sets of crustal faults (Kanamori and Stewart, 1978; Butler *et al.*, 1979; Kikuchi and Fukao, 1985; Kikuchi and Kanamori, 1986, 1991). Large non-double-couple (NDC) components of the long-period source mechanisms and their apparent disparity from first-motion observations are also explained through the occurrence of subevents on faults generating different focal mechanisms (Frohlich, 1994; Kikuchi *et al.*, 1993; Antolik *et al.*, 2000).

Recently, two large earthquakes, the 14 November 2001 Kunlun fault earthquake and the 3 November 2002 Denali fault earthquake, occurred along continental strike-slip fault zones dominated by oblique convergence (Fig. 1). In this article, we analyze these two important earthquakes using teleseismic *P*-wave data to derive a rupture history that may help us to understand the factors controlling the rupture initiation and complex behavior of large strike-slip earthquakes. In addition, we compare their source parameters with other large strike-slip events associated with different tectonic regimes.

Tectonic Setting and Seismicity

Denali Fault System (Central Alaska)

The 3 November 2002 Denali fault earthquake (M_w 7.9), which was preceded by a foreshock (M_w 6.7) on 23 October 2002, is the largest inland event ever recorded in central Alaska. The mainshock nucleated ~20 km east of the foreshock on the north-dipping Susitna Glacier reverse fault prior to rupturing more than 300 km to the east on the right-

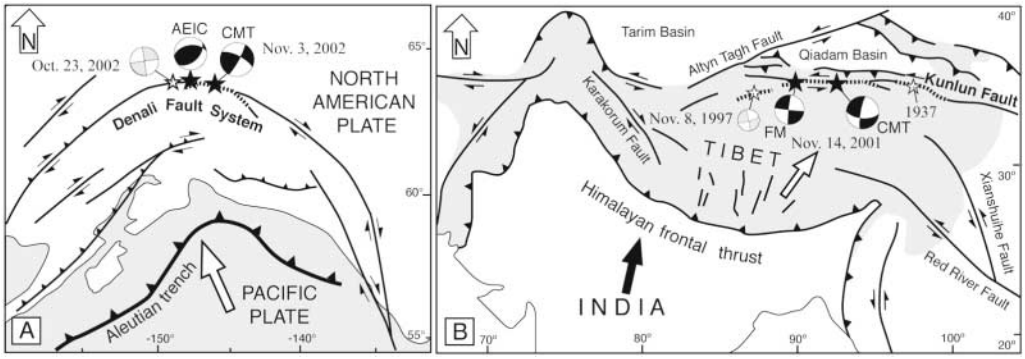

Figure 1. Simplified tectonic maps of our study areas: (A) Alaska-western Canada, and (B) Himalayan-Tibetan orogen. The arrows indicate relative plate motions. The surface ruptures for each large earthquake are shown by dashed lines. The *P*-wave first-motion mechanisms, CMT mechanisms, and corresponding locations are shown as solid stars. The location of the foreshock (23 October 2002) that occurred on the Denali fault, and large strike-slip earthquakes in 1937 and 1997 that occurred along the Kunlun fault are shown as open stars. CMT mechanisms and first-motion solutions of the Denali fault and Kunlun fault earthquakes are plotted in black. The first-motion mechanism of the Denali fault earthquake given by AEIC is based on data recorded on local stations. The first-motion mechanism for the Kunlun fault earthquake is based on teleseismic data.

lateral Denali fault system (Eberhart-Phillips *et al.*, 2003). A maximum right-lateral surface offset of 8.8 m occurred approximately 180 km east of the hypocenter (Eberhart-Phillips *et al.*, 2003) (Fig. 1A).

Across central Alaska, oblique convergence between the Pacific and North American plates is mainly partitioned between active subduction along the Alaska-Aleutian trench and right-lateral motion along crustal strike-slip faults such as the Denali fault (Plafker and Berg, 1994) (Fig. 1A). The Denali fault system follows an ancient suture between accreted lithotectonic terranes with a total displacement of 400 km (Lanphere, 1978) and displays a curvilinear geometry, implying a space problem at its apex (Redfield and Fitzgerald, 1993). Based on Holocene displacement, a slip rate of 10 $\pm$ 2 mm/yr is inferred for the central segment of the Denali fault that varies from east to west with earthquake recurrence times (T_r) ranging between 400 and 700 years for large events ($M > 7$) (Plafker *et al.*, 1993).

Prior to these large events in the fall of 2002, ongoing deformation caused minimal crustal seismicity along the Denali Fault with the largest event (M_w 5.8) occurring in 1996. The mechanisms of these earlier events indicated right-lateral motions along the Denali fault with the existence of compensating thrust systems as expected in a transpressive system (Ratchkovski and Hansen, 2002). Although the long-term seismic behavior of the fault is unknown, historical records and post-earthquake tree damage indicate a large earthquake (M 7.2) in 1912 that ruptured the Denali Fault (Doser, 2002; Carver *et al.,* 2004).

Kunlun Fault System (Northeast Tibet)

On 14 November 2001, a large earthquake (M_w 7.8) ruptured the left-lateral Kunlun strike-slip fault system in northeast Tibet and produced an asymmetric surface rupture toward the east that extends for more than 400 km (Fig. 1B). At the eastern segment, Xu *et al.* (2002) measured a maximum left-lateral offset of 7.6 m that is significantly less than the 16.3 m reported by Lin *et al.* (2002), which may represent a cumulative slip of more than one event. The observed surface offset near the hypocenter indicates a small 30-km-long strike-slip segment separated from the nearly 350-km segment of the Kunlun fault system by a 45-km-wide extensional step-over graben system (Xu *et al*., 2002). Based on the National Earthquake Information Center (NEIC) location, the earthquake initiated on the 30-km-long strike-slip segment near the extensional graben. However, there is no clear coseismic surface rupture visible across most of this 45-km-wide graben that might have occurred during the 2001 earthquake, but there is evidence of normal faulting marked by northwest-facing scarps with heights exceeding 1 m along a short extensional strand that bifurcates westward from the main strand of the Kunlun fault (Xu *et al.*, 2002).

The Kunlun fault system lies south of the Qiman Tagh active thrust system separating the Tibetan plateau to the south from the Qaidam Basin to the north. Although the present state of stress in the plateau is still poorly understood, ongoing motion of the Indian plate with respect to Siberia indicates convergence rates of up to 40 mm/yr, which is substantially accommodated within the plateau and its margins (Wang *et al.*, 2001). Structural mapping and receiver function studies reveal that the active oblique convergence has led to slip partitioning during which crustal extrusion is taken up by the Kunlun fault and crustal shortening by a decollement beneath the Kunlun range where the lithospheric mantle of Asia subducts southward (Meyer *et al.*, 1998; Kind *et al.*, 2002). Moho offsets detected from

double-pulse teleseismic *P*-wave arrivals (Zhu and Helmberger, 1998) and strong seismic anisotropy with the fast axis parallel to the Kunlun fault (McNamara *et al.,* 1994) suggest that the fault zone may extend deep in to the lithosphere (Lave *et al.*, 1996). The Kunlun fault system is a relatively young (<15 Ma) structure with a total horizontal displacement of less than 100 km (Yin and Harrison, 2000). Holocene offsets measured along the fault indicate an average slip rate of 11.5 ± 2 mm/yr (Van der Woerd *et al.*, 2002), which is consistent with Global Positioning System (GPS) data (Wang *et al.*, 2001). Offsets of channels and terraces have been interpreted to result from the occurrence of characteristic events that seem to be smaller ($M \sim 7.5$) but more frequent ($T_r \sim 420$ years) on the east than on the west ($M \sim 8$; $T_r \sim 900$ years) (Van der Woerd *et al.*, 2002).

In the region, seismicity is limited to a depth of approximately 15 km and defines a shallow seismogenic zone, which suggests aseismic deformation for the deeper section of the Kunlun fault zone. Overall, the fault-plane solutions imply a consistent pattern of pure left-lateral strike-slip faulting along the segments with strikes between west-southwest and north-northwest, oblique normal faulting along northeast–southwest-striking planes related to extensional steps, and thrusting along northwest–southeast-striking planes that are located within restraining bends and north of the Kunlun fault system. Prior to 14 November 2001, two large ($M > 7$) strike-slip earthquakes had ruptured neighboring segments of the Kunlun fault (Fig. 1B). In 1937, a $M \sim 7.5$ earthquake produced a 300-km-long surface break that stretches from 96° E to 100° E. Surface offsets indicated a nearly pure left-lateral mechanism with maximum horizontal displacements reaching up to 8 m (Molnar and Deng, 1984; Wu *et al.*, 1989). On 8 November 1997 another large (M_w 7.5) earthquake occurred on the westernmost segment of the Kunlun fault, between 86° E and 90° E, which was previously mapped by Tapponnier and Molnar (1977). Interferometric synthetic aperture radar (InSAR) results indicate a rupture length of about 170 km with 7 m of maximum slip (Peltzer *et al.*, 1999). From inversion of both surface and body waves, Velasco *et al.* (2000) obtained a left-lateral strike-slip mechanism similar to the Harvard Centroid Moment Tensor (CMT) solution and resolved a bilateral rupture that released most of the energy within the first 20 sec near the hypocenter.

Body-Wave Inversion

Data and Methodology

We used broadband teleseismic *P*-wave data recorded by the Global Seismic Network (GSN) and other stations archived at the Data Managementer Center of the Incorporated Research Institutions for Seismology (IRIS DMC). For each earthquake, we modeled more than 20 vertical-component *P*-wave displacement traces with good azimuthal coverage and high signal-to-noise ratios. Relative weights of observed records were chosen to enhance similar sampling from each quadrant and minimize the noise level. We did not include *SH* waves in our final results because at some distances the *SH* window was contaminated by other phases or the beginning of the *SH* wave was emergent and difficult to pick. We picked the first-motion *P* arrivals on the velocity traces and used that timing to align the data for the analysis. After the removal of the instrument responses, the data were integrated to displacement and bandpass filtered between 1 and 100 sec. Synthetic Green's functions were computed by using simple velocity models over a half-space including a crustal layer with a thickness of 35 km for central Alaska and 70 km for northern Tibet with a *P*-wave velocity (V_p) of 6.4 km/sec. We accounted for geometrical spreading and corrected for the attenuation time constant of $t_p^* = 1$ sec. Individual point sources were represented by a ramp time history, which fits the data best.

The inversion algorithm used in this study is based on a pulse-stripping method developed by Kikuchi and Kanamori (1982), which was later extended for variation in subevent mechanisms (Kikuchi and Kanamori, 1986, 1991). This method is also similar to the technique used by Lin *et al.* (2003) in a recent study of the Kunlun fault earthquake. By applying a multitime window inversion to the data, we derived the source-time function and the moment-release distribution along a fixed fault plane. Each pulse of moment release is located relative to the hypocenter on the prescribed fault plane with a given grid spacing. Moment release was allowed to occur within shallow crustal depths above 15–20 km and to vary along strike for several hundred kilometers. The moment, lag time, and location of the each subevent were determined with a positivity constraint, in order of decreasing moment, by minimizing the squared misfit between the observed residual and synthetic waveforms for all the stations simultaneously. This means that the reliability of solutions decreases in later iterations when misfits may eventually be compensated by "filling in" the fault plane with smaller subevents (Young *et al.*, 1989). The rupture velocity is not assumed but rather can be determined based on the timing and location of the pulses of moment release. We did impose a maximum rupture velocity of 4.5 km/sec for each inversion. We performed tests using different fault dimensions, grid spacings, and time windows, and we obtained very small variations in the spatial and temporal moment release for the largest subevents. For example, grid spacing on the prescribed fault of 5 or 10 km gave similar results. We estimate that our spatial resolution is at best 10–15 km. The observed moment pulses on each grid point were contoured by applying a smoothness constraint and then converted to slip by using the area of the largest asperity and its associated moment. During this step, we imposed zero slip at the lateral edges but free boundary conditions at the top and bottom of the fault plane.

As discussed by Kikuchi and Kanamori (1991), once the mechanism of the subevents are allowed to vary during each iteration, the inversion becomes unstable due to the

increase in the number of free parameters and results in a strong trade-off between timing, location, and focal mechanism of subevents. If no constraints are imposed on the focal mechanism, the solution becomes nonunique with many local minima of error and can be very path dependent (Young *et al.*, 1989; Kikuchi and Kanamori, 1991). The best way to eliminate this problem is to introduce constraints from other studies including strong-motion, surface-wave, geodetic, and geological data.

A discrepancy between first-motion polarities and the long-period focal mechanisms (Harvard CMT), significant changes in the surface offsets, and the dominant dip-slip mechanisms of some aftershocks illustrate the complex rupture characteristics of both the Denali fault and Kunlun fault earthquakes. Our initial attempts to invert the entire waveforms with a single mechanism showed that the initial portion of the *P* waves cannot be fit. A close look at the waveforms revealed a multiple-event nature in each case, which is characterized by an initial pulse followed by a much larger, later arrival. Amplitude ratios, and at some stations, polarity reversals between these two separated pulses, suggested a change in radiation pattern that can only be explained by composite rupture models involving a change in mechanism during the rupture.

To stabilize the inversion and at the same time to account for the smaller pulses with different source mechanisms, we focused on the initial complex portion of the waveforms. We tested a large range of double-couple mechanisms in a trial-and-error manner by determining the best slip model for each assumed mechanism (using the first 30–35 sec) and identified mechanisms that resulted in an improvement in the fit to the initial part of the *P* waveforms. The inversion duration was selected to enhance the waveform fit to the initial pulses and related depth phases. After we found a fault plane that improved the fit to the first 30–35 sec of data, we removed its contribution and inverted the residual waveforms for the total event duration (120 sec) using a fixed strike-slip mechanism that provides the lowest overall misfit to the data. At each step, the goodness of fit was estimated by the variance reduction (the squared sum of residual over the data power, subtracted from the perfect fit) and showed significant improvement for composite models. It is possible to implement more complex models with late-arriving pulses, but without a clear notion of the onset time and location, their contribution will be biased with somewhat arbitrary mechanisms, and in most cases resolution is not adequate to confirm their existence. We describe our results for each earthquake in the following sections.

The 2002 Denali Fault Earthquake

The 2002 Denali fault earthquake (M_w 7.9) is the largest recorded strike-slip earthquake to occur in central Alaska. The *P*-wave first-motion focal mechanism indicates that the rupture started as a thrust event, whereas the long-period Harvard CMT solution indicates a predominately strike-slip rupture (Fig. 2A). The mapped surface offset agrees with these results and shows an initially small thrust rupture followed by a much larger strike-slip rupture. Our initial study to model the *P*-wave displacement traces with a predominantly strike-slip mechanism showed significant misfit in the initial 35 sec, although it did a good job explaining the traces after 35 sec (Ozacar *et al.*, 2003). To understand the rupture initiation, we inverted for slip using different assumed fault-plane orientations for the initial 35 sec of the rupture as shown in Figure 2B. We find that the best-fitting result is for a subevent (M_w 7.3) with an almost pure thrust mechanism (strike slip, rake: 275°, 35°, 95°). The thrust fault plane gave a much better fit to the data than a strike-slip mechanism for the initial 35 sec (Fig. 2B). This subevent has a well-resolved pulse within the first 20 sec followed by a poorly resolved minor pulse, and it ruptured a 40-km-long fault segment (Figs. 2C and 3). We conclude that a thrust component is required by the teleseismic *P*-wave data to explain the early part of the rupture. The slip distribution resulting from a thrust mechanism shows an asperity (asperity 1 in Fig. 3) centered approximately 10 km east of the hypocenter where few aftershocks occurred (Fig. 3). The best-fitting fault plane with a 35° dip to the north corresponds well with the Susitna Glacier thrust fault, where 4.0 m of maximum vertical displacement was mapped (Eberhart-Phillips *et al.*, 2003).

After removing the thrust component from the *P*-wave displacement traces, the residual waveforms were modeled for the total event duration (120 sec) (Figs. 2 and 3). As shown in Figure 2B, the overall fit was better for a strike-slip mechanism that agrees with both the CMT solution and right-lateral surface offsets mapped across the Denali and Totschunda faults (Fig. 2B). The best fit was obtained by using a fault plane (strike, dip, rake: 295°, 55°, 170°) that suggests a dipping structure at depth consistent with oblique convergence (Fig. 2C). Our final model is shown in Figure 3. Strike-slip faulting started along the Denali fault just after the thrusting and propagated unilaterally to the east with an average rupture velocity of 3.2 km/sec. Our rupture velocity is similar to the rupture velocity of 3.3 km/sec determined by Dreger *et al.* (2004) using regional waveforms. The strike-slip part of the earthquake ruptured nearly 300 km in length with a moment magnitude of M_w 7.7. In our final model the largest episode of moment release (50–60 sec after rupture initiation) was contained in an energetic asperity (asperity 2 in Fig. 3) centered 150 km east of the hypocenter where right-lateral slip reached up to 8–9 m (Fig. 3). The location and maximum slip of this large asperity correlate well with large surface offsets. We observe low levels of seismic moment release between the two asperities that is difficult to resolve with the *P* waveforms. In contrast, the surface offset of 2–5 m along this region of the Denali fault is larger than we modeled with the teleseismic data.

The total seismic moment of our composite source model is 5.57×10^{20} N m (M_w 7.8) and agrees well with the moment calculated from strong-motion and GPS data

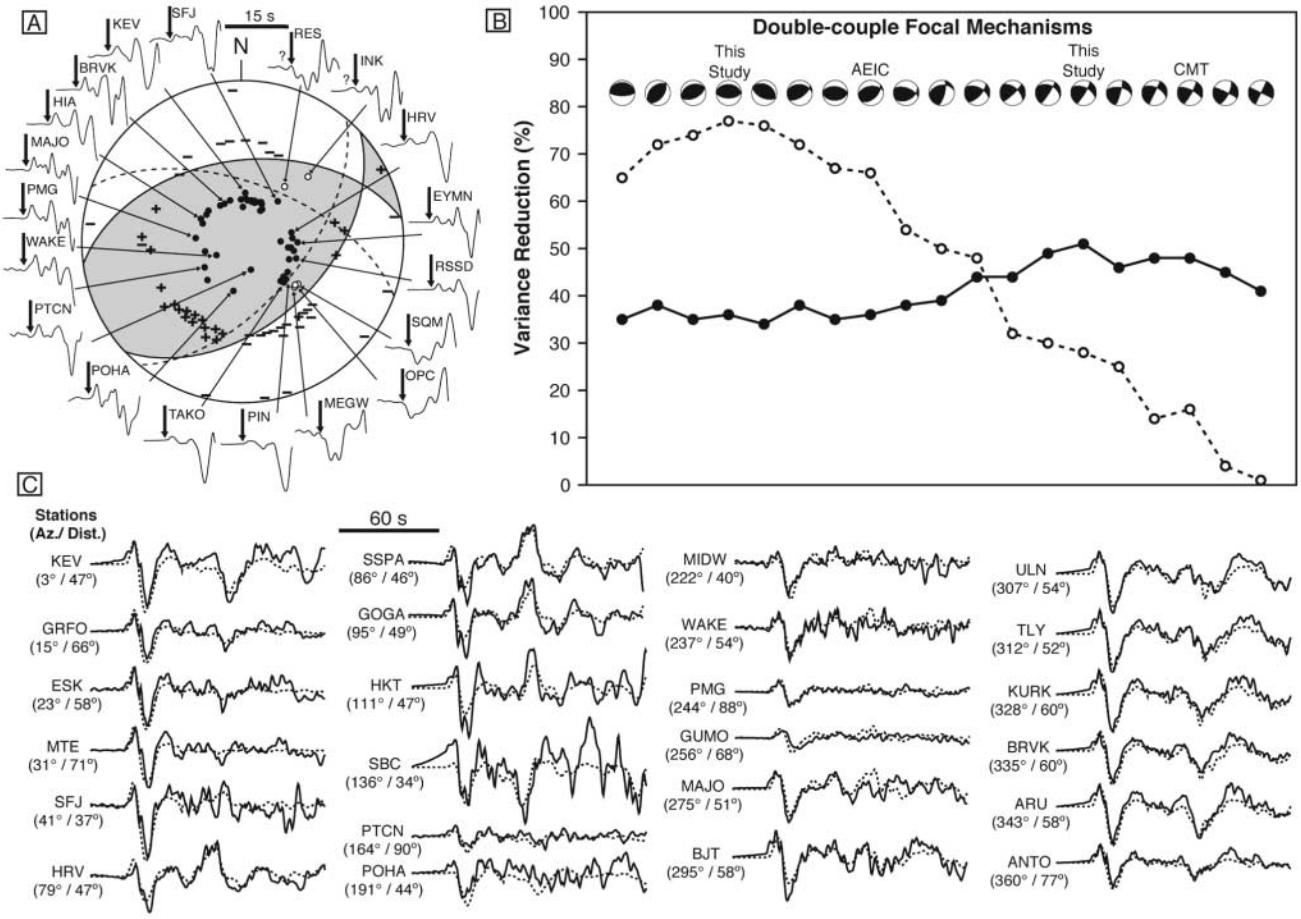

Figure 2. (A) The observed *P*-wave first-motion polarities of the Denali fault earthquake, plotted with the focal mechanism determined by AEIC (based on data recorded on local stations). The average focal mechanism used by Ozacar *et al.* (2003) is also plotted with dashed lines. The initial portions of the velocity traces are also shown with first-motion picks indicated with arrows. Solid (compression) and open (dilation) circles indicate polarities observed on regional and teleseismic stations. Plus (compression) and minus (dilation) signs indicate polarities observed on local stations by AEIC. (B) Variance reductions obtained for different time windows and focal mechanisms. The dashed line corresponds to the solutions for the initial 35 sec, and the solid line corresponds to the solutions for the total event duration (120 sec) using residual waveforms. (C) *P*-wave displacement traces (solid) plotted with synthetics (dashed) obtained from the inversion by using focal mechanisms with the highest variance reduction for each subevent. Amplitudes are scaled to the largest amplitude trace. The synthetic seismograms correspond to our preferred model shown in Figure 3.

(Eberhart-Phillips *et al.*, 2003; Hreinsdóttir *et al.*, 2003) but is lower than the long-period CMT solution (M_w 7.9). This event has a combined rupture length of 340 km. In general, the extent of the entire rupture is consistent with the distribution of relocated aftershocks (Ratchkovski *et al.*, 2003). The overall slip distribution and aftershock mechanisms are heterogeneous and suggest irregular conditions, such as the fault strength along the rupture zone. The zone of low seismic moment release just east of the hypocenter coincides well with the lack of aftershocks. Based on the spatial correlation of low bouguer gravity anomalies (Ozacar *et al.*, 2003) and fault-normal compression (Ratchkovski, 2003), this particular segment has been suggested to be weak.

The 2001 Kunlun Fault Earthquake

The complex *P* waveforms of the Kunlun fault earthquake also suggest two distinct moment pulses. Although the initial pulse is small and not significant with respect to the total moment release, it acts as the source of discrepancy observed between the first-motion mechanism and the centroid solution and is a key feature to understanding the initiation of rupture (Fig. 4). In this case the first motion is a left-lateral strike-slip mechanism, and the CMT solution has an oblique normal component (Fig. 4). We could not adequately fit the initial 20–30 sec of the *P*-wave displacement traces with either the first-motion focal mechanism or the

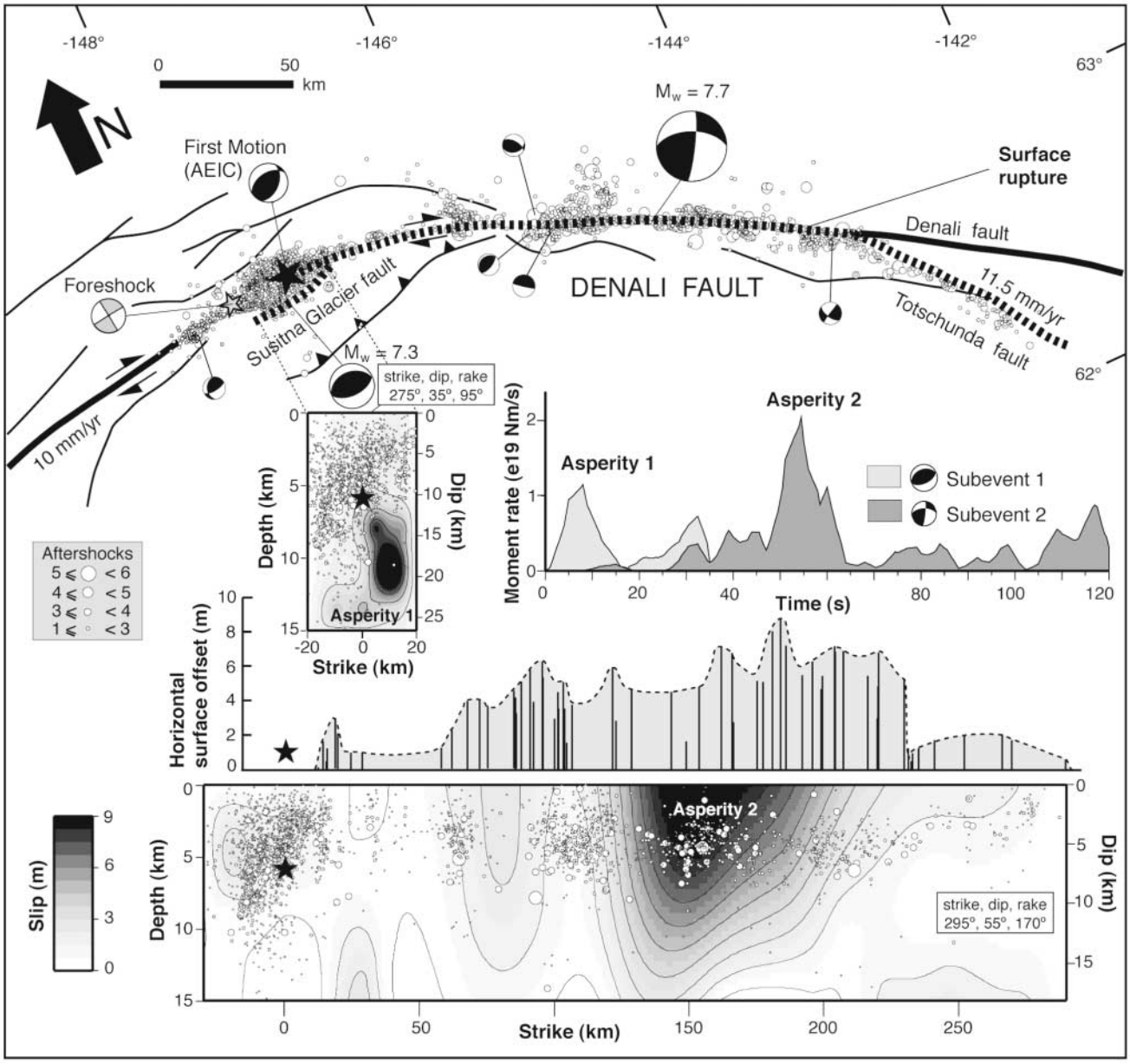

Figure 3. Map of the rupture area associated with the Denali fault earthquake with the observed horizontal surface displacements (Eberhart-Phillips *et al.*, 2003) and our preferred source model (subevent mechanisms, source-time functions, and slip distributions). The slip angle (rake) is fixed according to the fault-plane solutions of the subevents obtained from the inversion. Relocated aftershocks (2 months) are taken from Ratchkovski *et al.* (2003). Foreshock and aftershock mechanisms are from the CMT catalog. Filled stars indicate the hypocenter location.

CMT solution. We performed a grid search over a large range of fixed fault planes to determine the best-fitting double-couple mechanism for the first 30 sec of the *P* waveforms as shown in Figure 5A. We show two possible source models for the initial 30 sec (Fig. 5). In our one-subevent model we find the best fit to the data with an oblique focal mechanism having a normal fault component (strike, dip, rake: 255°, 40°, −30°) that results in the majority of the slip 20 km east of the hypocenter (Fig. 5A,B). The oblique normal fault plane clearly fits the data much better than a pure left-lateral strike-slip fault plane (Fig. 5A). However, based on the surface offset, there is a left-lateral strike-slip fault segment west of the hypocenter and an extensional graben with normal fault offsets to the east (Xu *et al.*, 2002). In addition, the *P*-wave first motions indicate a strike-slip mechanism for rupture initiation. Hence, in our two-subevent model we allowed for two possible fault planes during the first 30 sec of rupture. The two-subevent model, which we determined based on

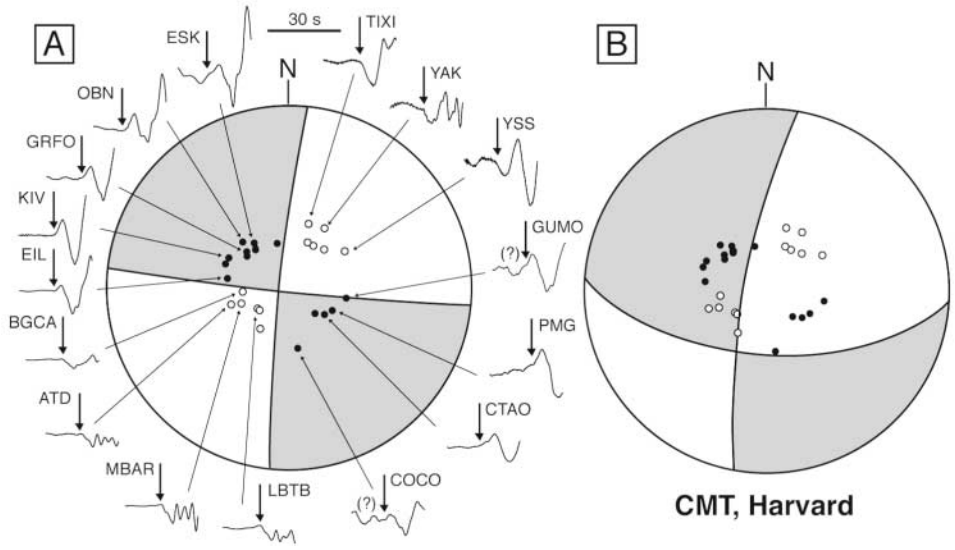

Figure 4. (A) The observed *P*-wave first-motion polarities and corresponding double-couple focal mechanism for the Kunlun fault earthquake plotted on a focal sphere. The initial portions of the *P*-wave velocity traces are also shown. First-motion picks are indicated with arrows. Stations showing compressional first motions are plotted as filled circles, and those showing dilatational first motions are plotted as open circles. Station GUMO is nodal to the fault plane with a very small first-motion and station COCO is too noisy to be picked reliably. (B) *P*-wave first-motion polarities, plotted with the long-period CMT solution. Polarities of stations with azimuths between 90° and 270° (e.g., PMG, CTAO, LBTB, MBAR, ATD, BGCA, etc.) do not fit the CMT solution.

trial-and-error modeling with both strike-slip and normal-fault mechanisms, provides a slightly better fit to the waveforms than the one-subevent case with a single oblique focal mechanism (Fig. 5A). In the two-subevent case the inversion results indicate strike-slip faulting (M_w 6.9) (strike, dip, rake: 95°, 75°, 15°) along a 30-km-long fault segment located west of the Taiyang Lake, and normal faulting (M_w 6.8) (strike, dip, rake: 250°, 40°, −40°) along a 40-km-long segment of a northwest-dipping fault located within the extensional step-over. This model suggests a bilateral rupture, in that faulting is occurring on both faults at the same time but in different locations. Based on the teleseismic *P*-wave data alone we cannot uniquely distinguish between these two models (one-subevent or two-subevent). However, the slip distributions of the two-subevent model agree well with the mapped surface geology and with the Kunlun fault rupture initiating at the intersection of the strike-slip segment and the extensional graben (Xu *et al.*, 2002). We agree with Antolik *et al.* (2004) that the Kunlun fault earthquake likely did rupture across the extensional graben at depth even though there is a gap in surface offset across part of the graben.

Once the initial pulse was modeled, we removed it from the data and inverted the residual waveforms for the total event duration (120 sec) by testing a series of double-couple mechanisms. There is very little difference in the residual waveform by using the one-subevent or two-subevent model. The results we show are for removing the two-subevent model largely based on the surface offset. The best fit was obtained with a left-lateral strike-slip mechanism having a fault plane (strike, dip, rake: 95°, 70°, −15°) that is consistent with the Harvard CMT solution and suggested a southward dip for the Kunlun fault (Fig. 6). According to the inversion results, the observable moment release along the strike-slip portion of the Kunlun fault began 40 sec after the first *P*-wave arrival and propagated eastward in a unilateral fashion with an average rupture velocity of 3.4 km/sec. We do not prescribe the rupture velocity but rather determine it based on the location and timing of the major pulse of moment release. This subevent ruptured a 350-km-long segment with a moment magnitude of M_w 7.7. The largest episode of moment release (65–80 sec) was contained in an energetic asperity centered 240 km east of the hypocenter, where left-lateral coseismic slip reached up to 9 m and surface offset reached nearly 8 m (Fig. 7). The average rupture velocity (3.4 km/sec) found in this study is similar to that obtained from Lin *et al.* (2003) of 3.4 km/sec and from Antolik *et al.* (2004) of 3.6 km/sec using similar body-wave data. This high rupture velocity found by all three studies is approaching the *S*-wave velocity in the crust but it is not as high (3.7–3.9 km/sec) as observed by Bouchon and Vallee (2003) using surface waves.

The overall pattern of slip distribution correlates well with the field observations (Xu *et al.*, 2002). There is very good agreement of our largest asperity location and slip with the maximum surface rupture (Xu *et al.*, 2002). We resolve very little slip on the Kunlun fault between the normal fault

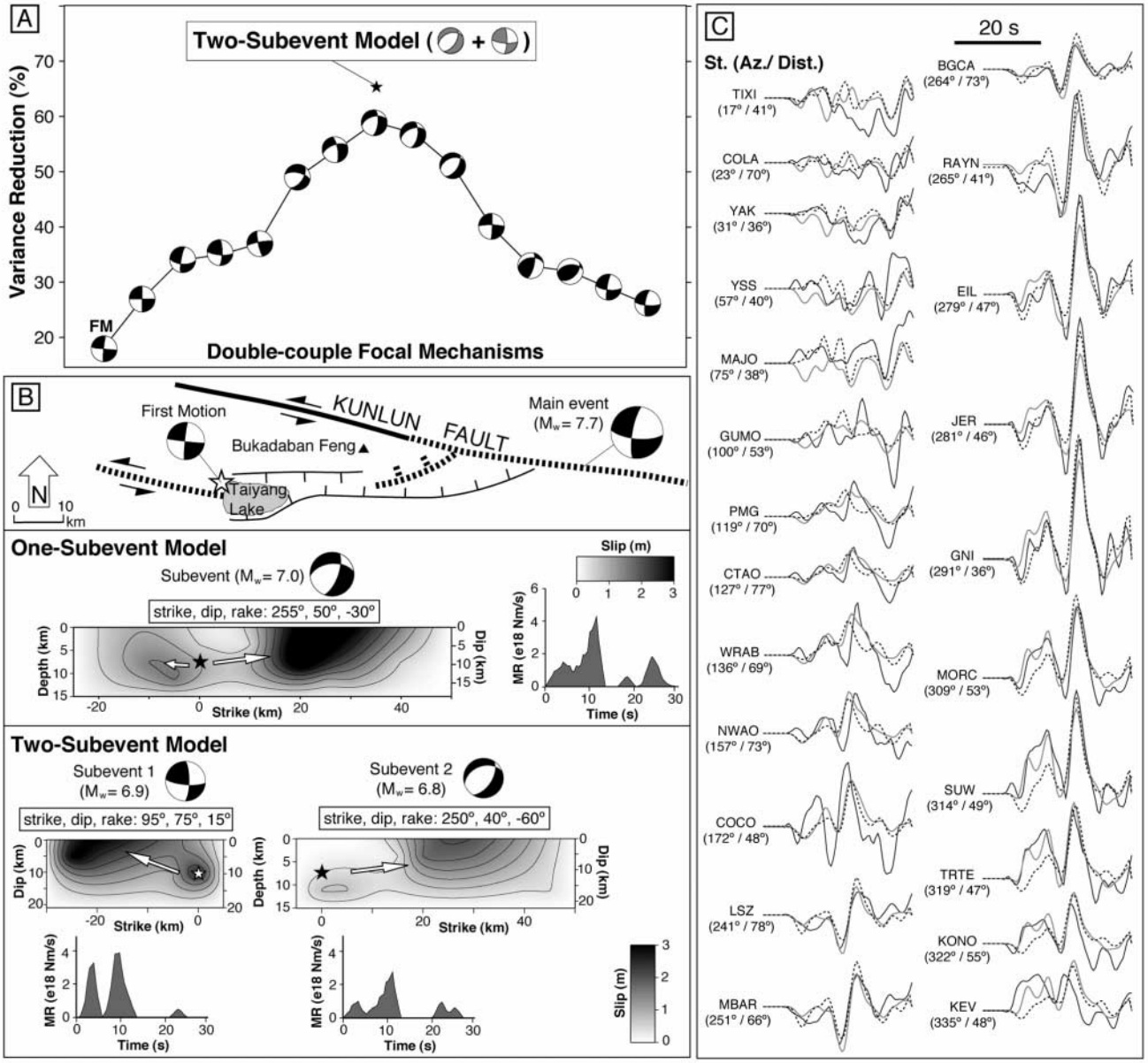

Figure 5. Results from our study of the initial 30 sec of the 2001 Kunlun fault earthquake. (A) Variance reductions obtained for the first 30 sec of the *P* waves by using one-subevent with a fixed fault plane (solid line) and for our preferred two-subevent model with two focal mechanisms (star). Note the improved fit using an oblique normal fault focal mechanism compared with a strike-slip mechanism. (B) Summary of our spatial and temporal inversion results for the initial 30 sec of rupture of the Kunlun fault earthquake. A map view of the western section of the Kunlun fault is shown at the top with the extent of the surface rupture (Xu *et al.*, 2002) shown by dashed lines. Fault-plane solutions, slip distributions, and source-time functions obtained for one-subevent and two-subevent models are shown at the bottom. Stars represent the hypocenter location and arrows point to the inferred rupture direction based on directivity. (C) *P*-wave displacement traces (solid) plotted with synthetics of one-subevent (dashed) and two-subevent (gray) models. Amplitudes are scaled to the largest-amplitude trace.

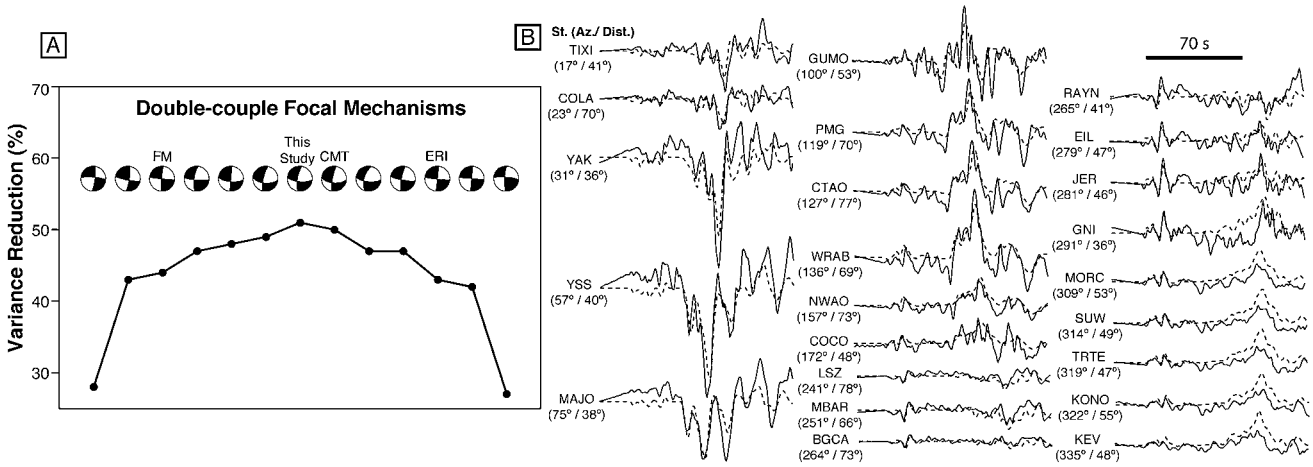

Figure 6. (A) Variance reductions obtained by testing different focal mechanisms to fit the residual waveforms (after removing the subevents in the initial 30 sec) for the Kunlun fault earthquake. We tested a large range of fault planes but show the variance reduction of a limited range of fault planes around our preferred mechanism. (B) *P*-wave displacement traces (solid) plotted with synthetic traces (dashed) generated by using our preferred model as shown in Figure 7 (the two-subevent model for the initial 30 sec of rupture and the strike-slip fault plane solution with highest variance reduction for the total event duration). Amplitudes are scaled to the largest amplitude trace.

component and approximately 150 km to the east. In contrast, there is as much as 2–4 m of surface offset along this region of the fault. Our composite source model gives a combined rupture length of 420 km and a total seismic moment of 4.55×10^{20} N m (M_w 7.7), which is slightly less than the long-period CMT solution (M_w 7.8). The location and timing of the largest asperity we identify (centered 240 km east of the hypocenter) is also very similar to the Antolik *et al.* (2004) study (250 km) but slightly further east than the Lin *et al.* (2003) study (220 km). Similar to the Denali fault earthquake, the Kunlun fault slip distribution is heterogeneous and suggests weaker faulting on the western section between the hypocenter and the major asperity. Most of the aftershocks clustered near the eastern tip of the fault where the fault bifurcates. For such a large event, very few aftershocks were recorded and the majority of them had thrust or normal mechanisms, revealing heterogeneous postevent stress conditions along the rupture zone.

Discussion

During the early twentieth century, large continental strike-slip earthquakes contributed dramatically to seismic hazard (1906 San Francisco, M_w 7.8; 1939 Erzincan, M_w 7.7; 1950 Assam, M_w 8.1), but few of them have been analyzed in detail because of limited data. In this respect, the Denali fault (M_w 7.9) and Kunlun fault (M_w 7.8) earthquakes stand out as being the two largest continental strike-slip events recorded by modern instrumentation. Body-wave inversion technique reveals very complex rupture histories for both earthquakes that include focal mechanism changes in the vicinity of the rupture nucleation and then major unilateral propagation along an anomalously long rupture zone with slip heterogeneity. In both cases the rupture nucleated on smaller faults before rupturing the main segment. The largest asperities and largest slip occurred more than 100 km from the rupture initiation for both earthquakes. Both earthquakes had very high apparent average rupture velocities of 3.2 km/sec and 3.4 km/sec for the Denali fault and Kunlun fault earthquakes, respectively. Both earthquakes occurred along faults that follow previous suture zones exhibiting different material properties on either side of the fault. One of the most striking features about both these earthquakes is the strong directivity and the long fault rupture. To infer the factors controlling directivity and rupture size, we compared source parameters of large strike-slip earthquakes worldwide to identify other strike-slip earthquakes with large unilateral ruptures and strong directivity.

Directivity

We searched the global catalogs for other large strike-slip earthquakes that have unilateral ruptures. Theoretically, the hypocenter derived from onset times of high-frequency *P* waves and the centroid obtained from analysis of long-period seismograms represent different characteristics of the earthquakes: the rupture initiation point and center of the total slip distribution, respectively (Smith and Ekström, 1997). For a large earthquake, unilateral rupture with the largest moment release far away from the hypocenter should produce the highest location shift compared with bilateral strike-slip events of similar magnitude (Fig. 8A). For example, the Kunlun fault and Denali fault earthquakes have a spatial separation of 214 and 139 km, respectively, be-

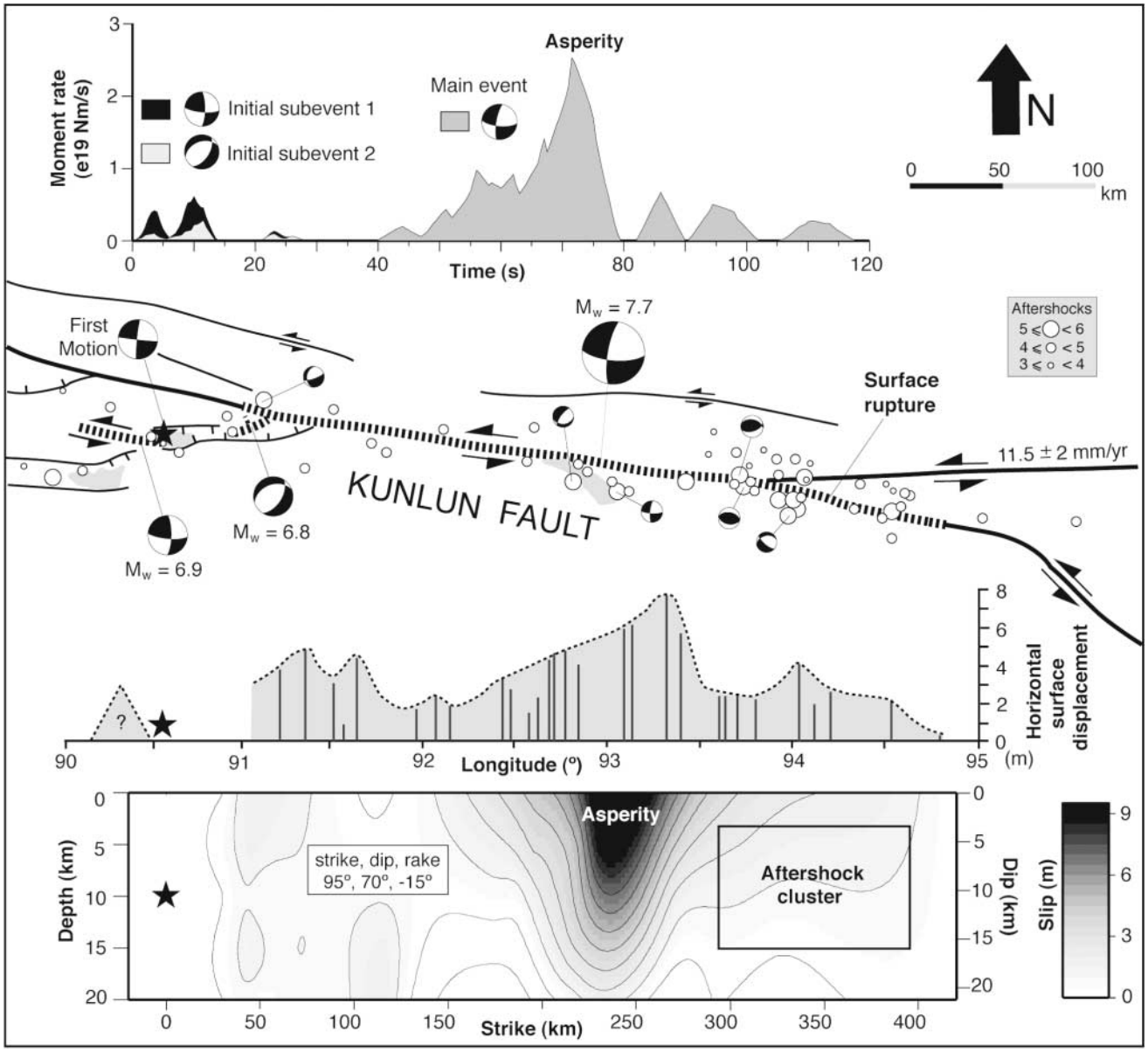

Figure 7. Map of the rupture area associated to the Kunlun fault earthquake with horizontal surface displacements (Xu *et al.*, 2002) and our preferred source model (focal mechanisms, source-time functions, and slip distribution of the main event). Slip angle (rake) is fixed according to the fault-plane solution of the main event obtained from the inversion. Aftershock locations are from USGS-NEIC and aftershock mechanisms are from CMT catalog. Filled stars indicate the hypocenter location.

tween their NEIC and centroid locations (Table 1). To identify other strike-slip earthquakes with large unilateral ruptures, the location shift between the hypocenter and centroid was calculated for all shallow (≤35 km) strike-slip events of $M_w \geq 6.5$ that are reported in the CMT and NEIC catalogs between 1976 and 2002. In practice, both location estimates have significant uncertainties, in part, related to lateral heterogeneity of the Earth (Smith and Ekström, 1996). To reduce the error in the data set, earthquakes for which the location shifts are inconsistent with the CMT solutions and tectonic setting were excluded.

In addition to the Denali fault and Kunlun fault earthquakes, we identified seven other earthquakes with unilateral ruptures (Table 1). All seven of the earthquakes are oceanic transform events that have smaller magnitudes ($6.5 \leq M_w \leq 7.0$) than the Denali fault and Kunlun fault earthquakes and location shifts of 60 to 134 km between the rupture initiation and the centroid location (Table 1, Fig. 8B). Among the plate-boundary tectonic setting, oceanic transform faults are of particular interest for this study because they are characterized by two different ages of material on either side of the fault trace. This difference parallels both

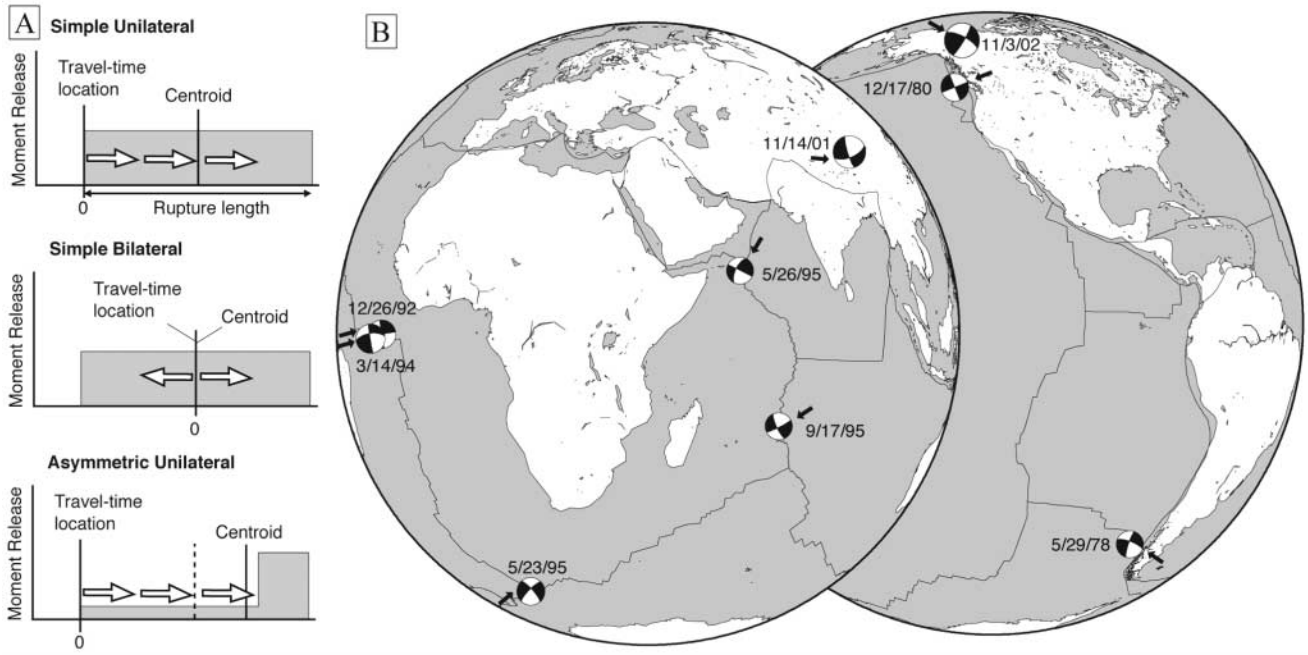

Figure 8. (A) Moment release versus distance from the initial break for simple unilateral, simple bilateral, and asymmetric unilateral ruptures (after Smith and Ekström, 1997). (B) Global locations and CMT solutions of large ($M_w \geq 6.5$) strike-slip earthquakes shallower than 35 km depth reported during the years 1976–2002 that show large (≥60 km) spatial separation between hypocenter (NEIC) and centroid (CMT) locations and inferred directivities consistent with tectonic setting and focal mechanisms. Arrows point to the inferred directivity, and solid lines represent the plate boundaries.

Table 1
Source Parameters of Large Unilateral Strike-Slip Earthquakes

			Epicenter (NEIC-PDE)*			Centroid (CMT catalog)				Location
Year	Month	Day	Long. (°)	Lat. (°)	Depth (km)	Long. (°)	Lat. (°)	M_0 (N m)	M_w	Shift (km)
1978	5	29	−79.41	−44.86	33	−81.00	−45.20	5.89×10^{18}	6.5	131
1980	12	17	−129.50	49.48	10	−130.54	49.37	1.40×10^{19}	6.7	76
1992	12	26	−19.29	−0.56	27	−18.76	−0.09	1.74×10^{19}	6.8	79
1994	3	14	−24.12	−1.39	10	−23.03	−0.88	4.11×10^{19}	7.0	134
1995	5	23	−3.15	−56.10	10	−2.14	−55.89	1.48×10^{19}	6.7	67
1995	5	26	57.93	12.13	10	57.55	11.75	6.08×10^{18}	6.5	60
1995	9	17	66.63	−17.25	10	66.06	−17.27	6.41×10^{18}	6.5	60
2001	11	14	90.54	35.95	10	92.91	35.80	5.90×10^{20}	7.8	214
2002	11	3	−147.69	63.74	10	−144.96	63.42	7.65×10^{20}	7.9	139

*NEIC-PDE, National Earthquake Information Center—*Preliminary Determination of Epicenter*.

the Denali fault and Kunlun fault settings. Simulations of dynamic rupture indicate the contrast in elastic properties and fault segmentation as two alternative explanations for the predominance of unilateral rupture (Cochard and Rice, 2000; McGuire *et al.*, 2002). In the absence of complex preexisting structural controls, material-property contrast provides a more likely explanation for the rupture directivity along transform faults. In contrast, both Denali and Kunlun faults display complex fault geometries along ancient suture zones that suggest rupture directivity may be a result of both fault segmentation and material contrasts across the fault.

Scaling Relations: A Global Review

Scaling of source properties for such large earthquakes is a very important issue for estimating the maximum possible earthquake size for a given region. Hence, we evaluate these two earthquakes with respect to scaling relations for large strike-slip events globally. Scatter in the global data set has led to a long-lasting debate on whether slip grows with the length or width of the fault (Scholz, 1982; Romanowicz, 1992). It is now widely recognized that sufficiently large crustal earthquakes rupture the entire width of the seis-

mogenic layer and grow only in one dimension. For very long ruptures, this theory predicts a rollover to constant slip (Bodin and Brune, 1996; Scholz, 1994) that agrees with new results from numerical modeling (Shaw and Scholz, 2001).

Until now, the scatter in the present global data set of strike-slip earthquakes has been largely explained in terms of systematic variations between different tectonic environments by distinguishing two classes of events. Most commonly, this distinction is made on the basis of plate boundaries (interplate versus intraplate) (Kanamori and Anderson, 1975; Scholz *et al.*, 1986) and recently made in terms of crust types (oceanic versus continental) (Romanowicz and Ruff, 2002). Although such distinctions capture the first-order effects, there is still a considerable amount of scatter.

Table 2
Source Parameters of Large ($M_0 > 10^{20}$ N m) Strike-Slip Earthquakes

Type	Location	Date	M_0	L	W	D	Ref.*
A	Fort Tejon (CA)	09-Jan-1857	7.00	380	12	5.1	1
A	San Francisco (CA)	18-Apr-1906	7.90	432	12	5.1	2
A	Erzincan (Turkey)	26-Dec-1939	4.50	350	12	3.6	1
A	Kastamonu (Turkey)	26-Nov-1943	2.60	280	14	2.2	2
A	Bolu (Turkey)	01-Feb-1944	2.40	175	12	3.8	1
A	Queen Charlotte (AK)	22-Aug-1949	11.00	440	15	5.6	1
A	Lituya Bay (AK)	10-Jul-1958	5.10	350	12	4.0	2
A	Sitka (AK)	30-Jul-1972	4.00	180	15	4.9	1
A	Guatemala	04-Feb-1976	3.10	257	13	3.1	2
A	Eureka (CA)	08-Nov-1980	1.12	120	*15*	2.1	3
A	New Zealand	25-May-1981	2.74	190	*15*	3.2	3
A	New Guinea	08-Feb-1987	1.11	90	*15*	2.7	3
A	Fiji Island	03-Mar-1990	3.01	220	*15*	3.0	3
A	Izmit (Turkey)	17-Aug-1999	1.70	135	12	3.5	4
B	Owens Valley (CA)	26-Mar-1872	2.90	108	15	6.0	2
B	Nobi (Japan)	27-Oct-1891	1.50	80	15	4.2	1
B	Kansu (China)	16-Dec-1920	12.00	220	20	9.1	2, 5
B	Kuyun (China)	10-Aug-1931	8.50	180	20	7.9	2, 5
B	Changma (China)	25-Dec-1932	2.80	116	*15*	5.4	2, 5
B	Assam (China)	15-Aug-1950	20.00	400	20	8.3	5
B	Darjung (China)	18-Nov-1951	4.60	200	10	7.7	2, 5
B	Gobi (Mongolia)	04-Dec-1957	18.00	300	20	10.0	2, 5
B	Luhuo (China)	06-Feb-1973	1.80	90	13	5.1	2, 5
B	Tangshan (China)	27-Jul-1976	1.76	70	24	3.5	2
B	Rudbar-Tarom (Iran)	20-Jun-1990	1.47	90	*15*	3.6	2
B	Luzon (Philippines)	16-Jul-1990	4.60	120	20	6.4	2
C	West Irian	12-Sep-1979	2.37	80	*15*	6.6	3
C	Alaska	30-Nov-1987	7.27	140	*15*	11.5	6
C	Alaska	06-Mar-1988	4.87	110	*15*	9.8	6
C	Macquarie Island	23-May-1989	15.00	220	20	11.4	7
C	Balleny Island	25-Mar-1998	17.00	320	15	11.8	8
C	SE Taiwan	03-May-1998	1.83	60	*15*	6.8	9
C	Ceram Sea	29-Nov-1998	4.48	90	*15*	11.1	9
C	Sulawesi	04-May-2000	2.44	70	*15*	7.7	9
C	S. Indian Ocean	18-Jun-2000	7.35	80	30	10.2	10
C	New Ireland	16-Nov-2000	15.60	180	30	9.6	11
C	Banda Sea	19-Oct-2001	1.86	65	*15*	6.4	12
C	Irian Java	10-Oct-2002	2.62	70	*15*	8.3	12
KF	Kunlun (Tibet)	07-Jan-1937	5.00	300	*15*	3.7	5
KF	Mayi (Tibet)	08-Nov-1997	2.40	170	15	3.1	13
KF	Kunlun (Tibet)	14-Nov-2001	**4.55**	420	15	2.4	14
DF	Denali (AK)	03-Nov-2002	**5.57**	340	15	3.6	14

M_0 (moment) in 10^{20} N m, D (displacement) in meters, L (length) and W (width) in kilometers. Displacement is determined using formula $M_0 = \mu LWD$, where $\mu = 3 \times 10^{11}$ dyne cm^2. Constant rupture width of 15 km is assumed for those, which are unknown (marked with italic characters). A, interplate; B, continental intraplate; C, oceanic intraplate; DF, Denali fault; KF, Kunlun fault; CA, California; AK, Alaska.

*(1) Fujii and Matsu'ura (2000); (2) Wells and Coppersmith (1994); (3) Pegler and Das (1996); (4) Reilinger *et al.* (2000); (5) Molnar and Deng (1984); (6) Lahr *et al.* (1988); (7) Das (1993); (8) Antolik *et al.* (2000); (9) Romanowicz and Ruff (2002); (10) Abercrombie *et al.* (2003); (11) Yagi and Kikuchi (2000); (12) Moment from CMT solution and length from aftershock distribution as given by NEIC catalog; (13) Ozacar *et al.* (2003); (14) Peltzer *et al.* (1999); (15) Results of this study.

In this study, large strike-slip earthquakes with reasonably well-defined source parameters (Table 2) were classified on the basis of their location with respect to plate boundaries and plate types into three categories: interplate, continental intraplate, and oceanic intraplate events (Fig. 9). We assumed a width of 15 km if no detailed studies of the seismogenic zone were available.

Despite the uncertainties, each category is characterized by distinct patterns in terms of source parameters, indicating that stresses are low for interplate, moderate for continental intraplate, and high for oceanic intraplate events (Fig. 10). In this respect, events associated with the Denali and Kunlun faults are anomalous and have an interplate signature rather than a continental intraplate signature. This overall weak fault behavior may be attributed to the strain-softening processes induced from preexisting suture zones.

Conclusions

Both the 2002 Denali fault and 2001 Kunlun fault earthquakes nucleated along small adjacent faults before propagating predominately unilaterally to the east along the main strand of a major strike-slip fault for hundreds of kilometers. Both earthquakes released most of their seismic moment along slip patches or asperities far from the hypocenter locations. Hence, these earthquakes did not initiate at the dominant asperity but rather the ruptures nucleated on smaller adjacent faults. The 3 November 2002 Denali fault earthquake began with initial thrusting (M_w 7.3) along a 40-km-long segment of the north-northwest-dipping Susitna Glacier fault and later ruptured a 300-km-long segment along the Denali and Totschunda faults with a right-lateral strike-slip mechanism (M_w 7.7). In contrast, the 14 November 2001 Kunlun fault earthquake nucleated along an extensional step-over with a bilateral rupture of a subevent pair consisting of 30-km-long strike-slip (M_w 6.9) and 40-km-long normal (M_w 6.8) faulting. The Kunlun fault earthquake then ruptured a 350-km-long segment along the Kunlun fault with a left-lateral strike-slip mechanism (M_w 7.7). The largest asperities and hence the largest moment release for both earthquakes occurred far from the rupture nucleation and corresponds well with the location and magnitude of the mapped surface offset.

To identify other strike-slip earthquakes with large unilateral ruptures, the location shift between the hypocenter and centroid was calculated for all shallow ($\leq$35 km) strike-slip events of $M_w \geq 6.5$ that are reported in the CMT and NEIC catalogs between 1976 and 2002. We identified seven additional strike-slip earthquakes that showed large location shifts between the hypocenters (NEIC) and centroids (CMT). All seven of these events were on oceanic transform faults. For these oceanic transform events the most likely reason for the long unilateral rupture propagation is the material contrasts (different age lithosphere) across the fault. For the Denali and Kunlun events, the preference of unilateral rupture may be due to both fault segmentation and material contrast across the fault.

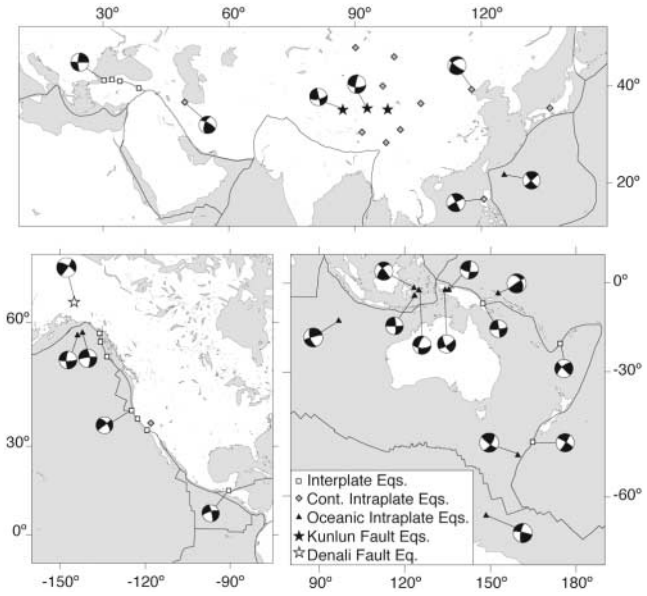

Figure 9. Maps showing the epicenter distribution of large crustal strike-slip earthquakes used in this study. Locations of events earlier than 1975 are taken from references listed in Table 2 and NEIC bulletins. For recent events, we used centroid locations and CMT solutions. Earthquakes are classified into three major categories (interplate, continental intraplate, and oceanic intraplate) based on their epicenter locations and relationship with the major plate boundaries.

Classification of large strike-slip earthquakes in terms of plate boundaries and crust types explains the observed scatter in source parameters and indicates that stresses are low for interplate, moderate for continental intraplate, and high for oceanic intraplate events. The Denali fault and Kunlun fault earthquakes correlate best with interplate events and thus appear to have ruptured relatively weak faults.

Acknowledgments

We used data from the GSN, a cooperative scientific facility operated jointly by IRIS, The United States Geological Survey (USGS), and the National Science Foundation (NSF). The facilities of the IRIS Data Management System, and specifically the IRIS Data Management Center, were used for access to waveform and metadata required in this study. We thank Natalia Ratchkovski, Douglas Christensen, and the staff of AEIC for providing the aftershock locations. We also benefited greatly from helpful comments of two anonymous reviewers and the assistance of Robert Fromm.

References

Abercrombie, R. E., M. Antolik, and G. Ekström (2003). The June 2000 M_w 7.9 earthquakes south of Sumatra: deformation in the India-Australia plate, *J. Geophys. Res.* **108,** 2018, doi 10.1029/2001JB000674.

Antolik, M., R. E. Abercrombie, and G. Ekström (2004). The 14 November 2001 Kokoxili (Kunlunshan), Tibet, earthquake: rupture transfer through a large extensional step-over, *Bull. Seism. Soc. Am.* **94,** 1173–1194.

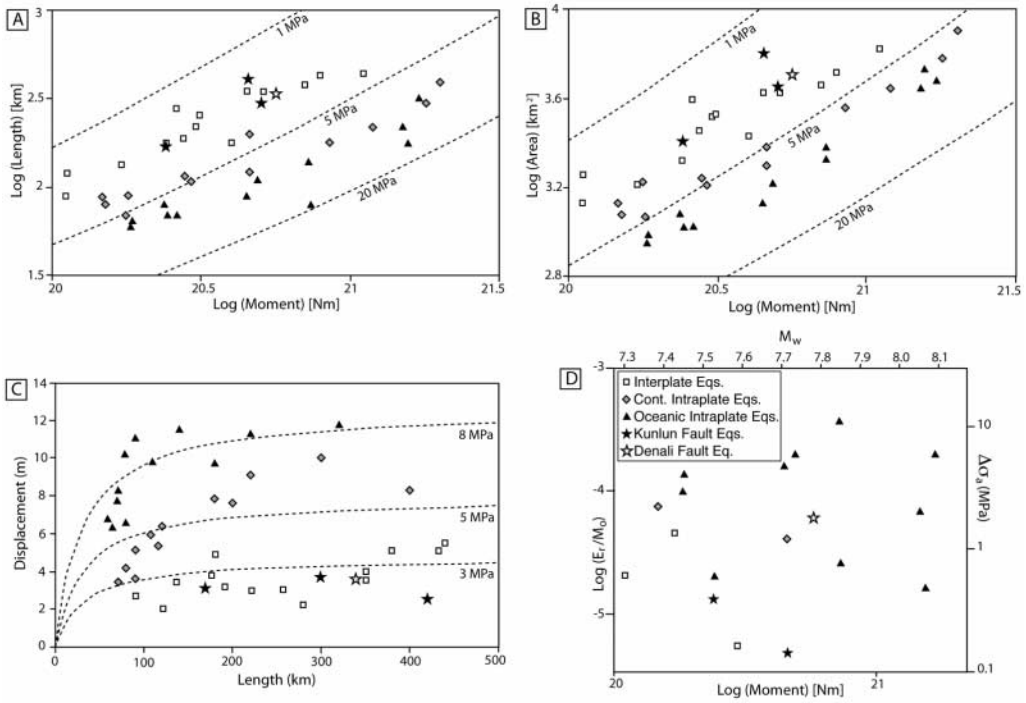

Figure 10. Plots of scaling relations for large crustal strike-slip earthquakes. Lines of equal stress drop (dashed) are calculated for a fault width (W) of 15 km by using $M_o = \mu LWD$ and $\Delta\sigma = 2\mu D/\pi\chi$, where M_o = seismic moment, $\mu = 3 \times 10^{11}$ dyne cm^2, L = rupture length, D = average displacement, $\Delta\sigma$ = stress drop, and χ (characteristic length) = $2LW/2W + L$ (Shaw and Scholz, 2001). (A) Rupture length as a function of seismic moment. (B) Rupture area (length × width) as a function of seismic moment. (C) Linear plot of displacement versus rupture length. (D) Radiated energy (E_r) to seismic moment (M_o) ratio, and apparent stress ($\Delta\sigma_a$) plotted as a function of M_o and moment magnitude (M_w). Broadband radiated energy (E_r) measurements are taken from USGS-NEIC. Apparent stress is calculated by using $\Delta\sigma_a = \mu E_r/M_o$.

Antolik, M., A. Kaverina, and D. S. Dreger (2000). Compound rupture of the great 1998 Antarctic plate earthquake, *J. Geophys. Res.* **105,** 23,825–23,838.

Bodin, P., and J. N. Brune (1996). On the scaling of slip with rupture length for shallow strike-slip earthquakes: Quasistatic models and dynamic rupture propagation, *Bull. Seism. Soc. Am.* **86,** 1292–1299.

Bouchon, M., and M. Vallée (2003). Observation of long supershear rupture during the M_s = 8.1 Kunlunshan (Tibet) earthquake, *Science* **301,** 824–826.

Butler, R., G. S. Stewart, and H. Kanamori (1979). The July 27, 1976 Tangshan, China earthquake: a complex sequence of intraplate events, *Bull. Seism. Soc. Am.* **69,** 207–220.

Carver, G., G. Plafker, M. Metz, L. Cluff, B. Slemmons, E. Johnson, J. Roddick, and S. Sorensen (2004). Surface rupture on the Denali fault interpreted from tree damage during the 1912 Delta River M_w 7.2–7.4 earthquake: Implications for the 2002 Denali fault earthquake slip distribution, *Bull. Seism. Soc. Am.* **94,** no. 6B, S58–S71.

Cochard, A., and J. Rice (2000). Fault rupture between dissimilar materials: I11-posedness, regularization, and slip-pulse response, *J. Geophys. Res.* **105,** 25,891–25,907.

Das, S. (1993). The Macquarie Ridge earthquake of 1989, *Geophys. J. Int.* **115,** 778–798.

Doser, D. I. (2002). Historical seismicity of the Denali fault system (abstract), *Eos Trans. AGU* **83,** (Fall Meet. Suppl.) S72F-1338.

Dreger, D. S., D. D. Oglesby, R. Harris, N. Ratchkovski, and R. Hansen (2004). Kinematic and dynamic rupture models of the November 3, 2002 M_w 7.9 Denali, Alaska, earthquake, *Geophys. Res. Lett.* **31,** L04605, doi 10.1029/2003GL018333.

Eberhart-Phillips, D., P. J. Haeussler, J. T. Freymueller, A. D. Frankel, C. M. Rubin, P. Craw, N. A. Ratchkovski, G. Anderson, G. A. Carver, A. J. Crone, T. E. Dawson, H. Fletcher, R. Hansen, E. L. Harp, R. A. Harris, D. P. Hill, S. Hreinsdóttir, R. W. Jibson, L. M. Jones, R. Kayen, D. K. Keefer, C. F. Larsen, S. C. Moran, S. F. Personius, G. Plafker, B. Sherrod, K. Sieh, N. Sitar, and W. K. Wallace (2003). The 2002 Denali fault earthquake, Alaska: a large magnitude, slip-partitioned event, *Science* **300,** 1113–1118.

Frohlich, C. (1994). Earthquakes with non-double-couple mechanisms, *Science* **264,** 804–809.

Fujii, Y., and M. Matsu'ura (2000). Regional difference in scaling laws of large earthquakes and its tectonic implication, *Pure Appl. Geophys.* **157,** 2283–2302.

Hreinsdóttir, S., J. T. Freymueller, H. J. Fletcher, and C. F. Larsen (2003). Coseismic slip distribution of the 2002 M_w 7.9 Denali fault earthquake, Alaska, determined from GPS measurements, *Geophys. Res. Lett.* **30,** 1670, doi 10.1029/2003GL017447.

Kanamori, H., and D. L. Anderson (1975). Theoretical basis of some empirical relations in seismology, *Bull. Seism. Soc. Am.* **65,** 1073–1095.

Kanamori, H., and G. S. Stewart (1978). Seismological aspects of the Guatemala earthquake of February 4, 1976, *J. Geophys. Res.* **83,** 3427–3434.

Kikuchi, M., and Y. Fukao (1985). Iterative deconvolution of complex body waves from great earthquakes—the Tokachi-Oki earthquake of 1968, *Phys. Earth Planet. Interiors.* **37,** 235–248.

Kikuchi, M., and H. Kanamori (1982). Inversion of complex body waves, *Bull. Seism. Soc. Am.* **72,** 491–506.

Kikuchi, M., and H. Kanamori (1986). Inversion of complex body waves—II, *Phys. Earth Planet. Interiors.* **43,** 205–222.

Kikuchi, M., and H. Kanamori (1991). Inversion of complex body waves—III, *Bull. Seism. Soc. Am.* **81,** 2335–2350.

Kikuchi, M., H. Kanamori, and K. Satake (1993). Source complexity of the 1988 Armenian earthquake: evidence for a slow after-slip event, *J. Geophys. Res.* **98,** 15,797–15,808.

Kind, R., X. Yuan, J. Saul, D. Nelson, S. V. Sobolev, J. Mechie, W. Zhao, G. Kosarev, J. Ni, U. Achaver, and M. Jiang (2002). Seismic images of crust and upper mantle beneath Tibet: evidence for Eurasian plate subduction, *Science* **298,** 1219–1221.

Lahr, J. C., R. A. Page, C. D. Stephens, and D. H. Christensen (1988). Unusual earthquakes in the Gulf of Alaska and fragmentation of the Pacific plate, *Geophys. Res. Lett.* **15,** 1483–1486.

Lanphere, M. A. (1978). Displacement history of the Denali fault system, Alaska and Canada, *Can. J. Earth Sci.* **15,** 817–822.

Lave, J., J. P. Avouac, R. Lacassin, P. Tapponnier, and J. P. Montagner (1996). Seismic anisotropy beneath Tibet: evidence for eastward extrusion of the Tibetan lithosphere? *Earth Planet. Sci. Lett.* **140,** 83–96.

Lin, A., B. Fu, J. Guo, Q. Zeng, G. Dang, W. He, and Y. Zhao (2002). Coseismic strike-slip and rupture length produced by the 2001 M_s 8.1 central Kunlun earthquake, *Science* **296,** 2015–2017.

Lin, A., M. Kikuchi, and B. Fu (2003). Rupture segmentation and process of the 2001 M_w 7.8 Central Kunlun, China, Earthquake, *Bull. Seism. Soc. Am.* **93,** 2477–2492.

McGuire, J. J., L. Zhao, and T. H. Jordan (2002). Predominance of unilateral rupture for a global catalog of large earthquakes, *Bull. Seism. Soc. Am.* **92,** 3309–3317.

McNamara, D. E., T. J. Owens, P. G. Silver, and F. T. Wu (1994). Shear wave anisotropy beneath the Tibetan plateau, *J. Geophys. Res.* **99,** 13,655–13,665.

Meyer, B., P. Tapponnier, L. Bourjot, F. Métivier, Y. Gaudemer, G. Peltzer, G. Shunmin, and C. Zhitai (1998). Crustal thickening in Gansu-Qinghai, lithospheric mantle, and oblique, strike-slip controlled growth of the Tibet plateau, *Geophys. J. Int.* **135,** 1–47.

Molnar, P., and Q. Deng (1984). Faulting associated with large earthquakes and the average rate of deformation in central and eastern Asia, *J. Geophys. Res.* **89,** 6203–6227.

Ozacar, A. A., S. L. Beck, and D. H. Christensen (2003). Source process of the 3 November 2002 Denali fault earthquake (central Alaska) from teleseismic observations, *Geophys. Res. Lett.* **30,** 1638, doi 10.1029/2003GL017272.

Pegler, G., and S. Das (1996). Analysis of the relationship between seismic moment and fault length for large crustal strike-slip earthquakes between 1977–1992, *Geophys. Res. Lett.* **23,** 905–908.

Peltzer, G., F Crampé, and G. King (1999). Evidence of nonlinear elasticity of the crust from the M_w 7.6 Manyi (Tibet) earthquake, *Science* **286,** 272–276.

Plafker, G., and H. C. Berg (1994). Overview of the geology and tectonic evolution of Alaska, in *The Geology of Alaska*, G. Plafker and H. C. Berg (Editors), Geological Society of America Boulder, Colorado, 989–1021.

Plafker, G., L. Gilpin, and J. C. Lahr (1993). Neotectonic map of Alaska, in *The Geology of North America*, vol. G-1, *Geology of Alaska*, plate 12, Geological Society of America, Boulder, Colorado.

Ratchkovski, N. A. (2003). Change in stress directions along the central Denali fault, Alaska after the 2002 earthquake sequence, *Geophys. Res. Lett.* **30,** 2017, doi 10.1029/2003GL017905.

Ratchkovski, N. A., and R. A. Hansen (2002). New constraints on tectonics of interior Alaska: earthquake locations, source mechanisms and stress regime, *Bull. Seism. Soc. Am.* **92,** 361–375.

Ratchkovski, N. A., R. A. Hansen, J. C. Stachnik, T. Cox, O. Fox, L. Rao, E. Clark, M. Lafevers, S. Estes, J. B. MacCormack, and T. Williams (2003). Aftershock sequence of the M_w 7.9 Denali fault, Alaska, earthquake of 3 November 2002 from the regional seismic network data, *Seism. Res. Lett.* **74,** no. 6, 743–752.

Redfield, T. F., and P. G. Fitzgerald (1993). Denali fault system of southern Alaska: an interior strike-slip structure responding to dextral and sinistral shear coupling, *Tectonics* **12,** 1195–1208.

Reilinger, R. E., S. Ergintav, R. Bürgmann, S. McClusky, Ö. Lenk, A. Barka, O. Gürkan, L. Hearn, K. L. Feigl, R. Çakmak, B. Aktug, H. Özener, and M. N. Töksoz (2000). Coseismic and postseismic fault slip for the 17 August 1999, $M = 7.5$, Izmit, Turkey Earthquake, *Science* **289,** 1519–1524.

Romanowicz, B. (1992). Strike-slip earthquakes on quasi-vertical transcurrent faults: inferences for general scaling relations, *Geophys. Res. Lett.* **19,** 481–484.

Romanowicz, B., and L. J. Ruff (2002). On moment-length scaling of large strike-slip earthquakes and the strength of faults, *Geophys. Res. Lett.* **29,** doi 10.1029/2001GL014479.

Scholz, C. H. (1982). Scaling laws for large earthquakes and consequences for physical models, *Bull. Seism. Soc. Am.* **72,** 1–14.

Scholz, C. H. (1994). A reappraisal of large earthquake scaling, *Bull. Seism. Soc. Am.* **84,** 215–218.

Scholz, C. H., C. A. Aviles, and S. G. Wesnousky (1986). Scaling differences between large interplate and intraplate earthquakes, *Bull. Seism. Soc. Am.* **76,** 65–70.

Shaw, B. E., and C. H. Scholz (2001). Slip-length scaling in large earthquakes: observations and theory and implications for earthquake physics, *Geophys. Res. Lett.* **28,** 2995–2998.

Smith, G. P., and G. Ekström (1996). Improving teleseismic event locations using a three-dimensional earth model, *Bull. Seism. Soc. Am.* **86,** 788–796.

Smith, G. P., and G. Ekström (1997). Interpretation of earthquake epicenter and CMT centroid locations, interms of rupture length and direction, *Phys. Earth Planet. Interiors.* **102,** 123–132.

Tapponnier, P., and P. Molnar (1977). Active faulting and tectonics in China, *J. Geophys. Res.* **82,** 2905–2930.

Van Der Woerd, J., P. Tapponnier, F. J. Ryerson, A. Meriaux, B. Meyer, Y. Gaudemer, R. C. Finkel, M. W. Caffee, Z. Guoguang, and X. Zhiqin (2002). Uniform postglacial slip-rate along the central 600 km of the Kunlun fault (Tibet), from ^{26}Al, ^{10}Be and ^{14}C dating of riser offsets, and climatic origin of the regional morphology, *Geophys. J. Int.* **148,** 356–388.

Velasco, A. A., C. J. Ammon, and S. L. Beck (2000). Broadband source modeling of the November 8, 1997, Tibet ($M_w = 7.5$) earthquake and its tectonic implications, *J. Geophys. Res.* **105,** 28,065–28,080.

Wang, Q., P. Zhang, J. T. Freymueller, R. Bilham, K. M. Larson, X. Lai, X. You, Z. Niu, J. Wu, Y. Li, J. Liu, Z. Yang, and Q. Chen (2001). Present-day crustal deformation in China constrained by global positioning system measurements, *Science* **294,** 574–577.

Wells, D. L., and K. J. Coppersmith (1994). New empirical relationships among magnitude, rupture length, rupture width, rupture area, and surface displacement, *Bull. Seism. Soc. Am.* **84,** 974–1002.

Wu, J., Y. Chen, and T. Lin (1989). Seismotectonics of Qinghai province, in *Lithospheric Dynamics Atlas of China,* State Seismological Bureau, China Cartographic Publishing House, Beijing, 55 pp.

Xu, X., W. Chen, W. Ma, G. Yu, and G. Chen (2002). Surface rupture of the Kunlunshan earthquake (M_s 8.1), northern Tibetan plateau, China, *Seism. Res. Lett.* **73,** 884–892.

Yagi, Y., and M. Kikuchi (2000). Preliminary results of rupture process for November 16, 2000 New Ireland region, Papua New Guinea earthquake, www.eic.eri.u-tokyo.ac.jp/yuji/PNG/index.html (last accessed September 2003).

Yin, A., and T. M. Harrison (2000). Cenozoic evolution of the Himalayan-Tibetan orogen, *Annu. Rev. Earth Planet. Sci.* **28,** 211–280.

Young, C. J., T. Lay, and C. S. Lynnes (1989). Rupture of the 4 February 1976 Guatemalan earthquake, *Bull. Seism. Soc. Am.* **79,** 670–689.

Zhu, L., and D. V. Helmberger (1998). Moho offset across the northern margin of the Tibetan plateau, *Science* **281,** 1170–1172.

Department of Geosciences
The University of Arizona
Tucson, Arizona, 85721-0077
ozacar@geo.arizona.edu
beck@geo.arizona.edu

Manuscript received 7 January 2004.